Available online at www.sciencedirect.com
SCIENCE DIRECT®
ELSEVIER
Journal of the European Ceramic Society 26 (2006) 1841–1844
ECRS
www.elsevier.com/locate/jeurceramsoc

Elimination of parasitic effects due to measurement conditions of $SrTiO_3$ thin films up to 40 GHz

Y. Iwazaki *, K. Ohta, T. Suzuki

Taiyo Yuden Co., Ltd., 5607-2 Nakamuroda, Haruna-machi, Gunma-gun, Gunma, Japan

Available online 8 November 2005

Abstract

Effective use of electromagnetic simulation software for evaluation of the microwave properties of dielectric thin films was demonstrated. The reliability of the high-frequency dielectric properties extracted from the measured S_{11} reflection coefficients with the aid of the electromagnetic simulation software is mainly limited by how accurately the measured parasitics are simulated. The need to correct the parasitic differences between the simulation and measurement was shown by the significant dependence of probe contact position on the obtained dielectric properties. The parasitic differences were represented by series and parallel correction admittances connected to the measured admittance and were effectively eliminated. The high-frequency dielectric properties of a highly crystalline $SrTiO_3$ (STO) thin film were investigated up to 40 GHz by using the measurement techniques developed. The permittivity (relative dielectric constant) of the STO thin film remained substantially constant at 265 up to 40 GHz, and the dielectric loss value was about 0.03 at 40 GHz.
© 2005 Elsevier Ltd. All rights reserved.

Keywords: Films; Dielectric properties; $BaTiO_3$ and titanates; Capacitors; Microwave

1. Introduction

Ferroelectric thin films show strong electric field-dependent nonlinear permittivity (relative dielectric constant) and are being extensively studied for applications in voltage-controlled tunable microwave devices, such as phase shifters,[1–3] resonators,[3] and tunable filters.[4] In particular, strontium titanate ($SrTiO_3$ or STO) and barium strontium titanate ($Ba_xSr_{1-x}TiO_3$ or BST) thin films are promising candidates for these applications. These BST thin films are generally used above the Curie temperature (T_c), in the paraelectric phase region, because of the need for low dielectric loss and sufficient tunability. Accordingly, $Ba_xSr_{1-x}TiO_3$ is typically used with x smaller than 0.7[1–3] for room temperature applications, while STO (x equals 0) is employed for cryogenic-temperature devices with high-T_c superconductors.[3–5] Metal–insulator–metal (MIM), that is, parallel-plate, tunable capacitors require relatively low control voltage, for example, below 10 V, for their operation compared to conventional planar-electrode tunable devices, which require hundreds of volts.[1–4] Moreover, the integration of tunable components on industrially important Si substrates can be easily achieved with MIM capacitors.[6–9] These properties make the MIM capacitor attractive for applications in consumer products. Several high-frequency characterization techniques of thin-film dielectrics in the MIM form have been proposed.[10–13] The main purpose of these measurement techniques is the removal of parasitics, such as parasitic inductance and resistance generated by the electrodes. However, there is little reliable data on the high-frequency dielectric properties of these tunable dielectric thin films, due to the difficulty of completely removing the parasitics.[8,9,12,14,15] Therefore, the development of accurate evaluation techniques for microwave dielectric properties is indispensable for optimizing tunable thin-film materials.

The aim of this study is to establish a reliable microwave measurement method for high-permittivity thin films by using electromagnetic simulation software and a vector network analyzer (VNA). With the techniques we developed, we accurately measured the high-frequency dielectric properties of highly crystalline STO thin films in a wide frequency range up to 40 GHz.

2. Experimental

STO thin films were deposited to a thickness of 120 nm at 650 °C in 2.7 Pa oxygen partial pressure, using ArF pulsed laser deposition (PLD). Thermally oxidized (SiO_2/1 μm) *n*-

* Corresponding author.

0955-2219/$ – see front matter © 2005 Elsevier Ltd. All rights reserved.
doi:10.1016/j.jeurceramsoc.2005.09.012

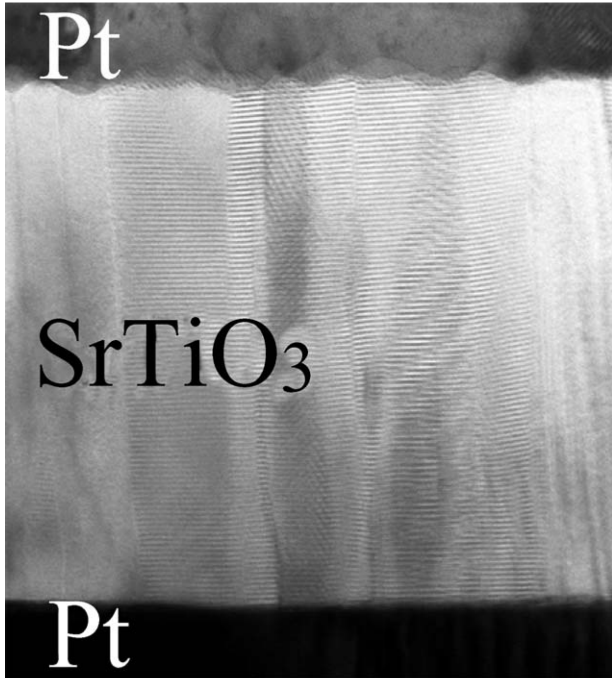

Fig. 1. Cross-sectional TEM image of STO thin film on $Pt/TiO_2/SiO_2/Si$ substrate.

Si (100) ($\rho \sim 6.7\,\mathrm{K\,\Omega\,cm}$) with a sputtered TiO_2 adhesive layer (2 nm) and a Pt electrode layer (250 nm) was used as the substrate. Electron beam-evaporated Pt was used for the top electrode. The dielectric and metal layers were etched with conventional photolithography to form the test structures. The film morphology and crystallinity were also evaluated by high-resolution transmission electron microscopy (HR-TEM). Fig. 1 shows a cross-sectional HR-TEM image of the STO thin film, indicating the well-crystallized columnar growth of the film on the $Pt/TiO_2/SiO_2/Si$ substrate. A VNA with a ground–signal–ground (GSG) probe calibrated with a standard calibration wafer was used to measure the one-port reflection coefficients S_{11} of the test structures at frequencies from 500 to 40 GHz. Care was paid for the probe contact condition on the electrode, such as probe contact position and contact pressure, and the enough measurement repeatability for the following analysis was confirmed. Electromagnetic field simulation software, which solves Maxwell's equations by a numeric simulation based on a finite element method, was used for simulating phase shifts and the magnitudes of the S_{11} parameters. Special care was paid to the mesh size of the finite element models to obtain fully converged data as far as possible.

3. Results and discussion

Fig. 2(a) schematically shows the device under test (DUT) structure containing an MIM capacitor of size 15 μm^2 defined by the top electrode area. The shape was almost identical with the previously reported test structure.[10–11] This structure was experimentally fabricated and was also modeled in the simulation software. The thin-film dielectric properties can be determined by matching the phase shift and the magnitude of the simulated

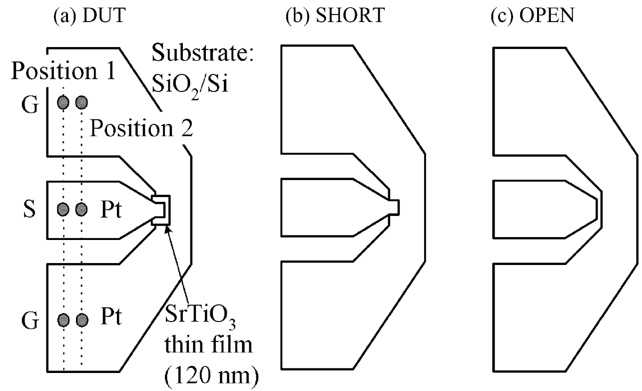

Fig. 2. Fabricated test structure shapes: (a) DUT, (b) SHORT and (c) OPEN.

S_{11} parameters with the measured ones.[13] However, their direct comparison inevitably leads to errors in the obtained dielectric properties due to some discrepancy in parasitics. One of the origins of the discrepancy is the measured parasitic inductance and resistance, which change depending on the measurement probe contact position. The generation of contact resistance between the probe and electrode metal is another source of discrepancy. These complicated additional parasitics make it difficult to create a reliable simulation model that correctly and completely simulates the measured parasitics. Therefore, some kind of correction is needed.

Correction of the parasitic differences is carried out using an admittance equivalent circuit shown in Fig. 3(a), where Y_{dut} and Y'_{dut} represent the measured and simulated admittances, and y_s and y_p represent series and parallel correction admittances, respectively. Y''_{dut} is the measured admittance of the DUT structure after correction. The parasitic differences were compensated for by the two correction admittances, y_s and y_p. Additional measurements and simulations were done for two different types of test structure, namely, the SHORT and OPEN structures shown in Fig. 2(b) and (c), respectively, to obtain the values of y_s and y_p. These results were used in the equivalent circuits shown in Fig. 3(b) and (c), where Y_{op}, Y'_{op}, Y_{sh}, and Y'_{sh}, respectively, represent the measured and simulated admittances for the OPEN

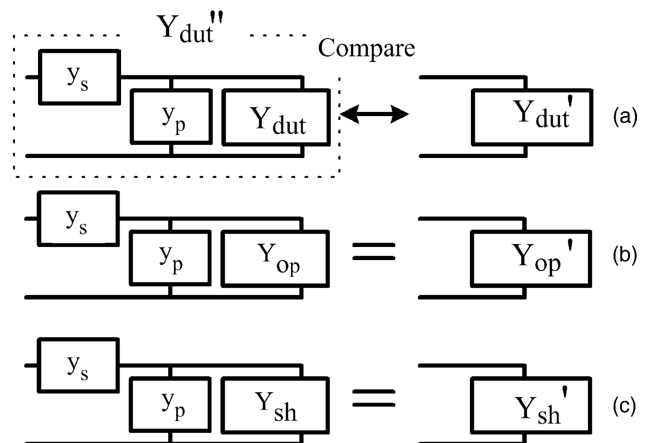

Fig. 3. Equivalent circuits used to correct the parasitic differences between the measurements and the simulations.

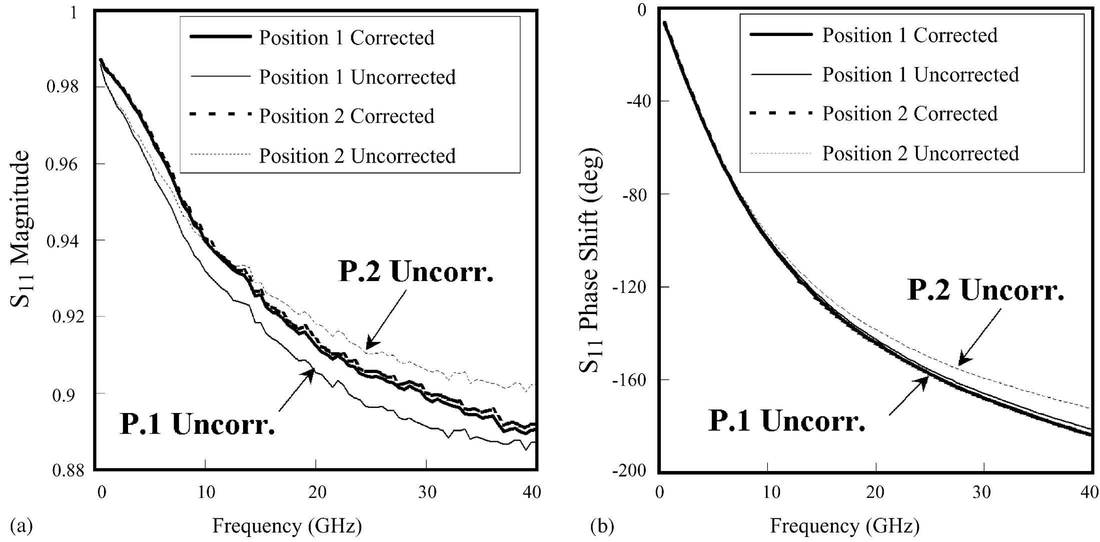

Fig. 4. Phase shifts and magnitudes of measured S_{11} parameters before and after correction at different probe contact positions.

and SHORT structures. From the equivalent circuits in Fig. 3(b) and (c), the following two equations were obtained:

$$\frac{y_s(y_p + Y_{op})}{y_s + y_p + Y_{op}} = Y'_{op} \quad (1)$$

$$\frac{y_s(y_p + Y_{sh})}{y_s + y_p + Y_{sh}} = Y'_{sh} \quad (2)$$

The correction admittances y_s and y_p as a function of frequency can be obtained by solving the simultaneous Eqs. (1) and (2) at each frequency. The OPEN and SHORT structures do not contain high-permittivity dielectric thin films, so the values of the correction admittances can be determined without considering the effects of such dielectric thin films, of which properties are unknown. The measured admittance Y_{dut} is corrected by using y_s and y_p as follows:

$$Y''_{dut} = \frac{y_s(y_p + Y_{dut})}{y_p + y_s + Y_{dut}} \quad (3)$$

Fig. 4(a) and (b) show the corrected and uncorrected magnitudes and phase shifts of the measured S_{11} parameters of the DUT structure at different probe contact positions labeled "Position 1" and "Position 2" shown in Fig. 2(a). The distance between the two positions was 27 μm. The uncorrected magnitude values at Position 1 in Fig. 4(a) are smaller than the corrected values because of the effect of the parasitic series resistance, which does not exist in the model, such as the contact resistance between the probe and the electrode. On the other hand, the uncorrected magnitude values at Position 2 are larger than the corrected values because the shorter measured effective length of the electrode makes the actual parasitic series resistance smaller than that used in the model. The uncorrected absolute values of the phase shift in Fig. 4(b), especially at Position 2, are smaller than the corrected values because of the reduced parasitic series inductance in the measurement. These differences are mainly corrected by the series admittance y_s. At Position 1, the estimated resistance value of y_s is −0.13 Ω, and the estimated inductance is 4.2 pH; at Position 2, the estimated values are 0.15 Ω and 19.5 pH, respectively.

The simulated S_{11} parameters were compared to the measured ones obtained after correcting for the parasitics to determine the thin-film dielectric properties. In the electromagnetic simulations, the simulated dielectric thin-film permittivity was varied from 160 to 280, and the dielectric loss was varied from 0 to 0.05 at each permittivity to match the simulated results with the measured ones. Fig. 5(a) and (b), respectively, show the frequency dispersion curves of the permittivity and the dielectric loss based on the optimized dielectric models at each frequency up to 40 GHz. The dotted lines and open marks in each figure show the results for the uncorrected measurements at the probe contact Positions 1 and 2. The dielectric properties without parasitic correction lie in the shaded areas in both the figures, depending on the probe contact position. The obtained frequency dispersion curves after correction are shown by the solid lines and the filled marks; these values converge into almost a single curve independent of the probe position, demonstrating the effectiveness of the correction of the generated parasitics due to the probe conditions and the ability to evaluate the thin-film dielectric properties over a wide frequency range. The measured permittivity of the STO thin film remained almost constant at about 265, and the dielectric loss gradually increased to about 0.03 as the frequency was increased to 40 GHz. The accuracy of these results depends on the measurement repeatability, the structural uniformity of the measured and simulated structures, and the simulation accuracy of the models. In particular, the simulation results contain inevitable errors as a result of the finite number of mesh elements in the model. These errors are estimated as ΔS_{mag} (error in the absolute value of the S_{11} parameter) of ±0.003–0.005 at 40 GHz, corresponding to a dielectric loss error $\Delta \tan\delta$ of ±0.01–0.016 and a permittivity error $\Delta\varepsilon_r$ of ±1.2–2.0. The obtained results inevitably contain some errors, but this kind of simulation error will be eliminated in the near future as computer processing power advances.

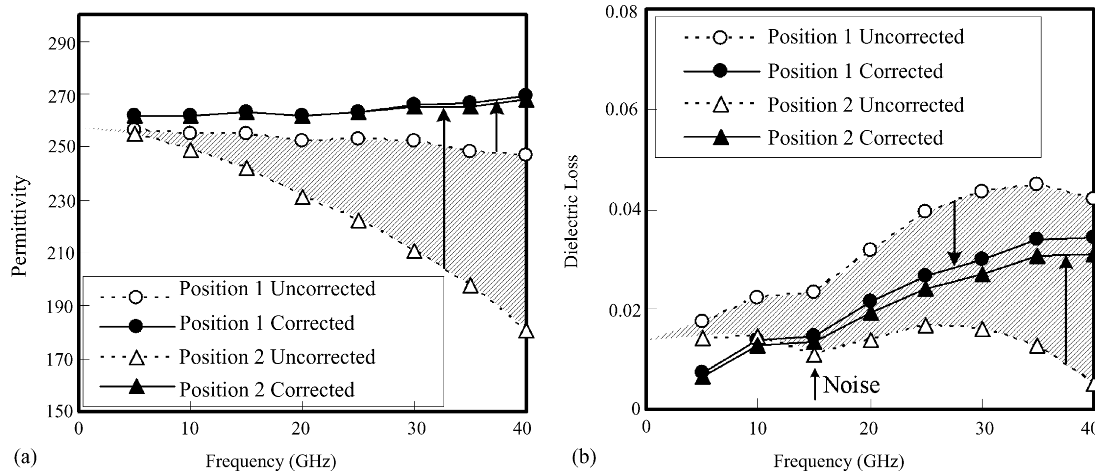

Fig. 5. Permittivities and dielectric losses of the STO thin film as a function of frequency before and after correction.

4. Conclusions

In conclusion, we have shown reliable measurement techniques for the evaluation of the microwave properties of dielectric thin films with the aid of electromagnetic simulation software. The importance of correcting the parasitic difference between the measured and simulated results was demonstrated by showing the dependence of probe contact position on the obtained dielectric properties. The parasitic differences were effectively corrected by introducing correction admittances and equivalent circuits. The permittivity of the highly crystalline STO thin film remained almost constant at 265 (±2) up to 40 GHz, and the dielectric loss was about 0.03 (±0.016) at 40 GHz. As far as we know, the varying parasitics due to the measurement conditions were not treated properly in previous studies. In this report, we have shown an effective correction method by which these parasitic effects can be effectively removed in evaluating the thin-film dielectric properties.

Acknowledgement

This work was supported by the Science and Technology Promotion Adjustment Fund for "Ceramics Integration" from the Ministry of Education, Culture, Sports, Science and Technology of Japan.

References

1. Wu, H.-D. and Barnes, F. S., Doped $Ba_{0.6}Sr_{0.4}TiO_3$ thin films for microwave device applications at room temperature. *Integr. Ferroelectr.*, 1998, **22**, 291–305.
2. Keuls, F. W. V., Mueller, C. H., Miranda, F. A., Romanofsky, R. R., Horwitz, J. S., Chang, W. *et al.*, Thin film $Ba_xSr_{1-x}TiO_3$ Ku- and K-band phase shifters grown on MgO substrates. *Integr. Ferroelectr.*, 2000, **28**, 49–61.
3. Keuls, F. W. V., Romanofsky, R. R., Mueller, C. H., Warner, J. D., Candy, C. L., Ramesh, R. *et al.*, Current status of thin film (Ba,Sr)TiO_3 tunable microwave components for RF communications. *Integr. Ferroelectr.*, 2001, **34**, 165–176.
4. Christen, H.-M., Silliman, S. D., Harshavardhan, K. S., Knauss, L. A., Zhao, Z. and Zaki, K. A., Optimization of materials and design for electrically tunable microwave filters. *Integr. Ferroelectr.*, 1999, **24**, 247–256.
5. Dalberth, M. J., Stauber, R. E., Price, J. C. and Rogers, C. T., Improved low frequency and microwave dielectric response in strontium titanate thin films grown by pulsed laser ablation. *Appl. Phys. Lett.*, 1998, **72**, 507–509.
6. York, R. A., Nagra, A. S., Periaswamy, P., Auciello, O., Streiffer, S. K. and Im, J., Synthesis and characterization of $(Ba_xSr_{1-x})Ti_{1+y}O_{3+z}$ thin films and integration into microwave varactors and phase shifters. *Integr. Ferroelectr.*, 2001, **34**, 177–188.
7. Vorobiev, A., Rundqvist, P., Khamchane, K. and Gevorgian, S., Silicon substrate integrated high Q-factor parallel-plate ferroelectric varactors for microwave/millimeterwave applications. *Appl. Phys. Lett.*, 2003, **83**, 3144–3146.
8. Baniecki, J. D., Laibowitz, R. B., Shaw, T. M., Duncombe, P. R., Neumayer, D. A., Kotecki, D. E. *et al.*, Dielectric relaxation of $Ba_{0.7}Sr_{0.3}TiO_3$ thin films from 1 mHz to 20 GHz. *Appl. Phys. Lett.*, 1998, **72**, 498–500.
9. Kim, T. G., Oh, J., Kim, Y., Moon, T., Hong, K. S. and Park, B. W., Crystallinity dependence of microwave dielectric properties in (Ba,Sr)TiO_3 thin films. *Jpn. J. Appl. Phys.*, 2003, **42**, 1315–1319.
10. Ikuta, K., Umeda, Y. and Ishii, Y., Measurement of high-frequency dielectric characteristics in the mm-wave band for dielectric thin films on semiconductor substrates. *Jpn. J. Appl. Phys.*, 1995, **34**, L1211–L1213.
11. Ikuta, K., Umeda, Y. and Ishii, Y., Upper-bound frequency for measuring mm-wave-band dielectric characteristics of thin films on semiconductor substrates. *Jpn. J. Appl. Phys.*, 1998, **37**, 210–214.
12. Ma, Z., Becker, A. J., Polakos, P., Huggins, H., Pastalan, J., Wu, H. *et al.*, RF measurement technique for characterizing thin dielectric films. *IEEE Trans. Electr. Dev.*, 1998, **45**, 1811–1816.
13. Hamano, T., Towner, D. J. and Wessels, B. W., Relative dielectric constant of epitaxial $BaTiO_3$ thin films in the GHz frequency range. *Appl. Phys. Lett.*, 2003, **83**, 5274–5276.
14. Dube, D. C., Baborowski, J., Muralt, P. and Setter, N., The effect of bottom electrode on the performance of thin film based capacitors in the gigahertz region. *Appl. Phys. Lett.*, 1999, **74**, 3546–3548.
15. Kim, Y., Oh, J., Kim, T.-G. and Park, B., Influence of the microstructures on the dielectric properties of ZrTiO4 thin films at microwave-frequency range. *Jpn. J. Appl. Phys.*, 2001, **40**, 4599–4603.